Supplementary Material

A monolithic integrated ultra-flexible all-solid-state supercapacitor based on polyaniline conducting polymer

Fan Li[a], Jun Liu[b], Yao Ma[b], Zhenzhen Shang[a], Qing-an Huang[a], Xiaodong Huang[a*]

[a]*Key Laboratory of MEMS of the Ministry of Education, Southeast University, Nanjing 210096, China*

[b]*National Key Laboratory of Electromagnetic Environmental Effects and Electro-optical Engineering, Army Engineering University, Nanjing 210007, China*

* Electronic mail: xdhuang@seu.edu.cn

The specific areal capacitance of single electrode (C_s), energy density (E) and power density (P) could be extracted from the CV and GCD curves by the following equations:

$$C_s = \frac{\oint IdU}{Av\Delta U} \qquad \text{S1}$$

where v is the CV scan rate, ΔU (~ 1.2 V) is the potential window and A is the electrode area.

$$C_s = \frac{2It}{A\Delta U} \qquad \text{S2}$$

where I is the constant discharge current, t is the discharge time, ΔU (~ 1.2 V) is the potential window and A is the electrode area.

$$E = \frac{C_s \Delta U^2}{4h} \qquad \text{S3}$$

where C_s is the specific areal capacitance of single electrode extracted from equation S2, ΔU (~ 1.2 V) is the potential window and h is the whole thickness of the device including the current collectors, electrodes, electrolyte and support.

$$P = \frac{E}{t} \qquad \text{S4}$$

Table S1 Comparison of several typical membranes used as the SC supports

	Cost	Weight	Porosity	Flexibility
Polycarbonate (PC)	×	✓	×	✓
Polyethylene terephthalate (PET)	✓	✓	×	✓
Carbon nanotube (CNT) or graphene	×	✓	✓	✓
Polydimethyl-siloxane (PDMS)	✓	✓	×	✓
Polyimide (PI)	✓	✓	×	✓
Nylon	✓	✓	✓	✓

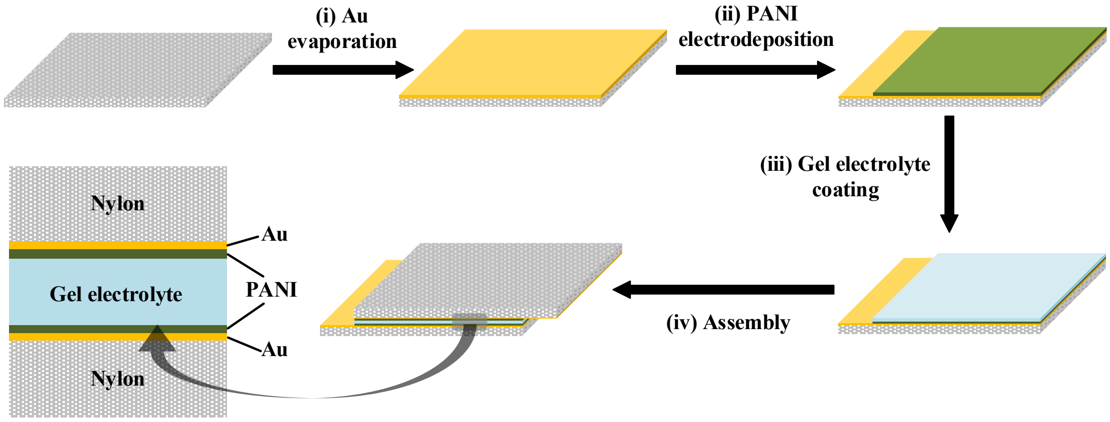

Fig. S1. Fabrication processes of the reference SC.

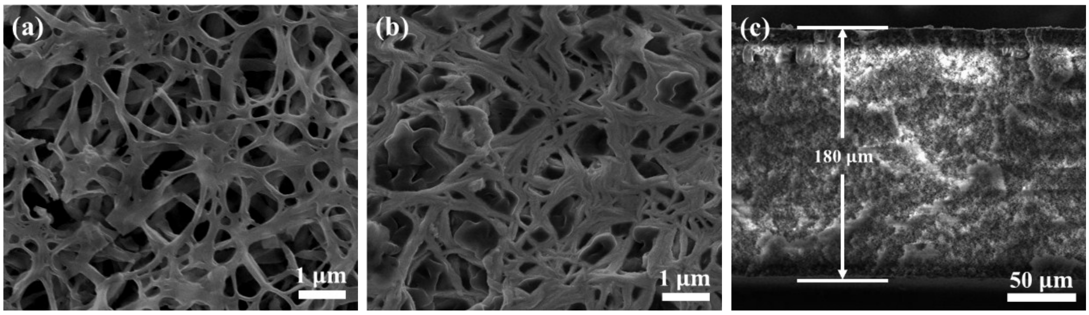

Fig. S2. Plan-view SEM images of the nylon membrane (a) before and (b) after Au deposition; (c) cross-sectional SEM image of the fresh nylon membrane.

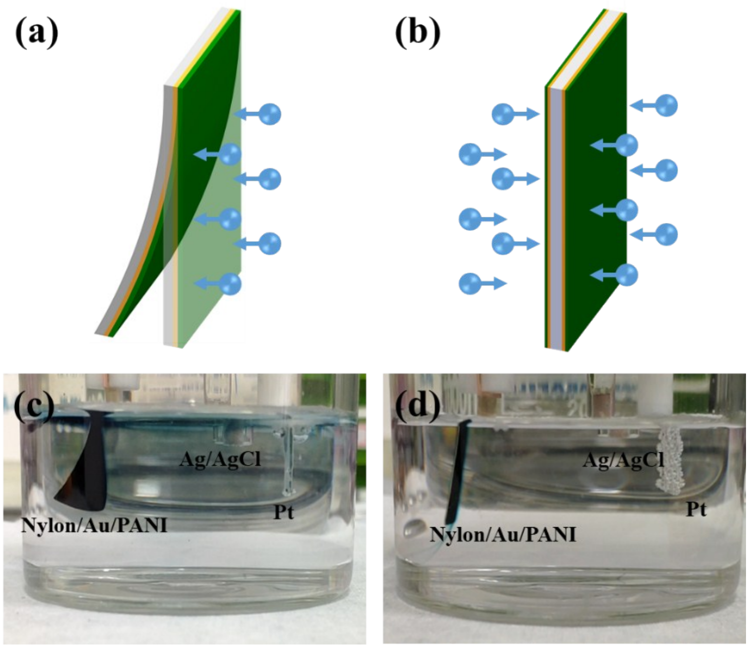

Fig. S3. Schematic diagrams of the PANI electrodeposition on (a) only one side and (b) both sides of the nylon membrane. Photographs of the PANI electrodeposition on (c) only one side and (d) both sides of the nylon membrane.

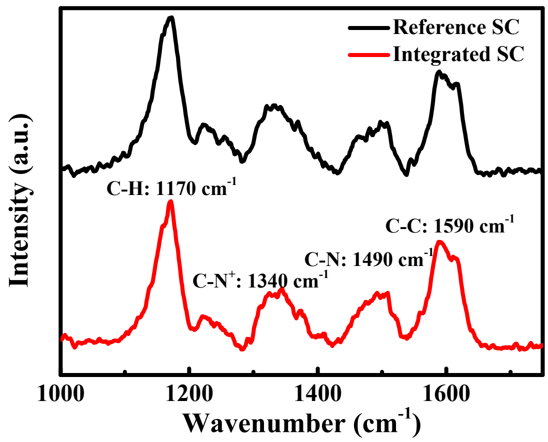

Fig. S4. Raman spectra of the PANI films for the integrated and reference SCs.

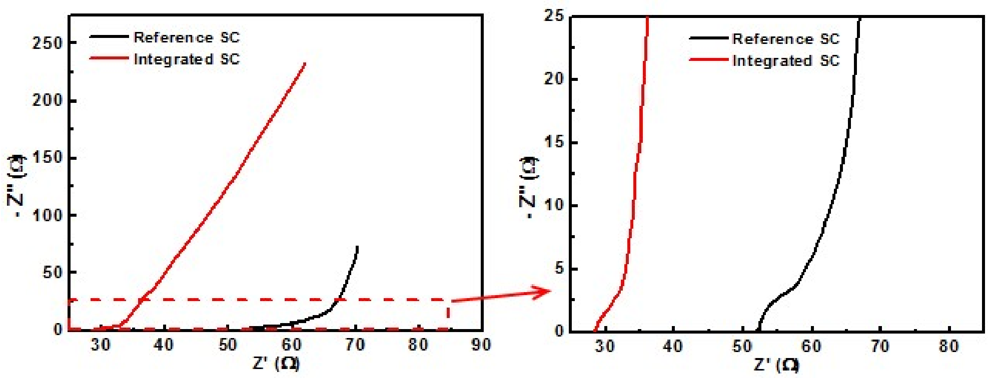

(a) (b)

Fig. S5. (a) Nyquist plots of the integrated and reference SCs before cycling and (b) the enlarged Nyquist plots in the rectangular area of Fig. S5(a). As seen in the figure, the equivalent series resistance (ESR) can be extracted from the intersection between the EIS curve and x axis (at y=0). The charge transfer resistance (R_{ct}) corresponds to the diameter of the semicircle of the EIS curve at high-to-medium frequencies, and the integrated SC shows much smaller diameter than the reference one, suggesting its much lower R_{ct}.

(a) (b)

Fig. S6. (a) Nyquist plots of the SCs after cycling and (b) the enlarged Nyquist plots in the rectangular area of Fig. S6(a). Compared with the EIS curves before cycling (as seen in Fig. S5), the EIS curves after cycling degrade for both the integrated and reference SCs. However, the reference SC exhibits much more severe degradation than the integrated one and the ESR before and after cycling is 52.1 Ω and 62.0 Ω for the reference SC and 28.6 Ω and 31.2 Ω for the integrated SC, corresponding to 19.0% and 9.1% degradation respectively.

Table S2 Performance comparison between the present and previous reported works. Note that the item of capacitance (mF cm^{-2}) represents the specific areal capacitance of single electrode. Regarding the items of power density and energy density, the whole SC volume is used for calculating the energy and power densities in this work and Ref [16-18], while only the electrode volume is used for calculation in Ref [2, 14] and the whole volume except the support is used for calculation in Ref [15].

Composition	Potential range (V)	Capacitance (mF cm^{-2})	Power density	Energy density	Discharge rate (mA cm^{-2})	Capacitance retention
EG-PANI [1]	0~1	80.4	4.14 mW cm^{-2}	0.003 mWh cm^{-2}	1	90.24% (1000)
PANI [2]	-0.6~0.6	131.3	140 mW cm^{-3}	21.8 mWh cm^{-3}	1	95.2% (2000)
PAN/G/MWCNTs/PPS [3]	0~2	300	4.44 mW cm^{-2}	0.123 mWh cm^{-2}	4	98% (2000)
PANI/MLG [4]	0~0.7	60	0.15 mW cm^{-2}	0.01 mWh cm^{-2}	0.85	100% (1000)
NG/PANI [5]	0~1	584.7	9.999 mW cm^{-2}	0.051 mWh cm^{-2}	20	108% (2000)
HGC-PANI [6]	0~1	~450	600 mW cm^{-3}	9.4 mWh cm^{-3}	10	90% (3000)
CNF/CNTs/PANI [7]	0~0.8	67.31	1.92 mW cm^{-2}	0.006 mWh cm^{-2}	4	90% (5000)
PANI [8]	-0.2~0.8	15	~0.3 mW cm^{-2}	0.001 mWh cm^{-2}	0.3	90% (1000)
$Ni_3V_2O_8$ @ PANI [9]	0~1.6	52.8	7.06 mW cm^{-2}	0.016 mWh cm^{-2}	3	88% (20000)
CNFs/CNTs/PANI [10]	-0.2~0.8	626	2.5 mW cm^{-2}	0.05 mWh cm^{-2}	5	71% (10000)
CNT/PANI [11]	0~0.7	184.6	1.18 mW cm^{-2}	0.008 mWh cm^{-2}	5	95% (500)
PANI/CNT/EVA [12]	0~0.8	192.3	1200 mW cm^{-2}	8.35 mWh cm^{-2}	5	66.4% (3000)
PHE-PANI [13]	0~0.8	131	0.4 mW cm^{-2}	0.012 mWh cm^{-2}	1	83.7% (5000)
(RGO/CNTs)@PANI [14]	0~0.8	36.7 F cm-3	200 mW cm^{-3}	0.8 mWh cm^{-3}	2 A cm^{-3}	80.6% (2000)
ACM/MWCNT/PANI [15]	0~2.5	2.2 F cm-3	500 mW cm^{-3}	1.13 mWh cm^{-3}	30	80.3% (5000)
a-Fe_2O_3/PANi [16]	0~1.8	236.8	67 mW cm^{-3}	0.31 mWh cm^{-3}	10 A g^{-1}	80.3% (5000)
PANI/MWCNT/PDMS [17]	0~0.8	2.1 F cm-3	185 mW cm^{-3}	0.09 mWh cm^{-3}	6	95% (500)
PANI [18]	0~0.7	718	1.47 mW cm^{-3}	0.051 mWh cm^{-3}	0.5	96% (13000)
Reference SC	-0.6~0.6 V	308.5	17.4 mW cm^{-3} (1.2 mW cm-2)	0.2 mWh cm^{-3} (0.02 mWh cm^{-2})	2	83.7% (6500)
Integrated SC	-0.6~0.6 V	341.7	73.9 mW cm^{-3}	1.7 mWh cm^{-3}	2	92.8% (6500)

	(1.4 mW cm^{-2})	(0.03 mWh cm^{-2})

Reference:

[1] O. Sadak, M.U.A. Prathap, S. Gunasekaran, Facile fabrication of highly ordered polyaniline e exfoliated graphite composite for enhanced charge storage, Carbon N. Y. 144 (2019) 756–763. doi:10.1016/j.carbon.2018.12.062.

[2] Z. Huang, Y. Ma, L. Wang, Flexible all-solid-state supercapacitors based on polyaniline orderly nanotubes array, Nanoscale. (2017) 193–200. doi:10.1039/c6nr07921k.

[3] M. Faraji, H.M. Aydisheh, Flexible free-standing polyaniline/graphene/carbon nanotube plastic films with enhanced electrochemical activity for an all-solid-state flexible supercapacitor device, New J. Chem. (2019) 4539–4546. doi:10.1039/c9nj00043g.

[4] G. De Souza, J. Scarmínio, P. Rog, A. De Siervo, C. Sekhar, F. Rouxinol, Flexible metal-free supercapacitors based on multilayer graphene electrodes, Electrochim. Acta. 285 (2018). doi:10.1016/j.electacta.2018.07.223.

[5] Y. Zou, Z. Zhang, W. Zhong, W. Yang, Hydrothermal direct synthesis of polyaniline, graphene/polyaniline and N-doped graphene/ polyaniline hydrogels for high performance flexible supercapacitors, J. Mater. Chem. A. (2018) 9245–9256. doi:10.1039/c8ta01366g.

[6] Y. Qu, C. Lu, Y. Su, D. Cui, Y. He, C. Zhang, M. Cai, F. Zhang, X. Feng, X. Zhuang, Hierarchical-graphene-coupled polyaniline aerogels for electrochemical energy storage, Carbon N. Y. 127 (2018) 77–84. doi:10.1016/j.carbon.2017.10.088.

[7] J. Tang, S. Qin, X. Xu, J. Hong, C. Zhao, W. Lu, D.-Z. Chen, F. Wang, X. Ouyang, J. Liu, X. Xiong, A high performance all-solid-state flexible supercapacitor based on carbon nanotube fiber/carbon nanotubes/polyaniline with a double core-sheathed structure, Electrochim. Acta. 283 (2018) 366–373. doi:10.1016/j.electacta.2018.06.158.

[8] K. Wang, H. Wu, Y. Meng, Y. Zhang, Z. Wei, Integrated energy storage and electrochromic function in one flexible device: An energy storage smart window, Energy Environ. Sci. 5 (2012) 8384–8389. doi:10.1039/c2ee21643d.

[9] X. Liu, J. Wang, G. Yang, In situ growth of the $Ni_3V_2O_8$@PANI composite electrode for flexible and transparent symmetric supercapacitors, ACS Appl. Mater. Interfaces. 10 (2018)

20688–20695. doi:10.1021/acsami.8b04609.

[10] S. Tan, J. Li, L. Zhou, P. Chen, J. Shi, Modified carbon fiber paper-based electrodes wrapped by conducting polymers with enhanced electrochemical performance for supercapacitors, Polymers (Basel). (2018). doi:10.3390/polym10101072.

[11] M. Chen, Y. Kang, H. Chen, Q. Li, F. Cai, S. Zeng, Electrochemical fabrication of carbon nanotube/polyaniline hydrogel film for all-solid-state flexible supercapacitor with high areal capacitance, J. Mater. Chem. A. 3 (2015) 23864–23870. doi:10.1039/c5ta05937b.

[12] X.P. G, D.B. Kong, Q. Huang, L. Cao, P. Zhang, H.J. Lin, Z.D. Lin, H. Yuan, In situ growth of a high-performance all-solid-state electrode for flexible supercapacitors based on a PANI/CNT/EVA composite, Polymers (Basel). (2019). doi:10.3390/polym11010178.

[13] R. Jia, H. Du, X. Zhang, Z. Chen, D. Chen, Stretchable and compressible supercapacitor with polyaniline on hydrogel electrolyte, Electrochem. Soc. 165 (2018) 3792–3798. doi:10.1149/2.0481816jes.

[14] D. Liu, P.C. Du, W.L. Wei, H.X. Wang, Q. Wang, P. Liu, Skeleton/skin structured (RGO/CNTs)@PANI composite fiber electrodes with excellent mechanical and electrochemical performance for all solid-state symmetric supercapacitors, J. Colloid Interface Sci. 513 (2018) 295-303. doi:10.1016/j.jcis.2017.11.027.

[15] C.Q. Lin, J. Jie, L.X. Wei, W.G. Chao, W. Xi, Y.C. Yang, High-performance stretchable supercapacitors based on intrinsically stretchable acrylate rubber/MWCNTs@conductive polymer composite electrodes, J. Mater. Chem. A. 6(2018) 4432-4442. doi:10.1039/c7ta11173h.

[16] C.M. Qing, L.S. Rong, S.D. Jian, T. Li, Y.Z. Kun, Y. Jin, Hierarchical nanostructured α-Fe_2O_3/polyaniline anodes for high performance supercapacitors, Electrochim. Acta. 269(2018) 21-29. doi:10.1016/j.electacta.2018.02.144.

[17] B. M. Sadeeq, C.M. Qing, L.S. Rong, L.X. Hong, M.K. Cheng, S.D. Jian, T. Li, T.Y. Xiang, Y.Z. Kun, Y. Jin, Y.M. Hao, Z.Y. Xiang, Z.Y. Fan, Z.Z. Shou, Water surface assisted synthesis of large-scale carbon nanotube film for high-performance and stretchable supercapacitors, Adv. Mater. 26(2014) 4724-4729. doi: 10.1002/adma.201401196.

[18] L.F. Tang, P.Q. Min, W.J. Chen, An all-in-one self-healable capacitor with superior

performance, J. Mater. Chem. A. 6(2018) 2500-2506. doi: 10.1039/c7ta10323a.